Vectorcardiographic Loop Alignment and the Measurement of Morphologic Beat-to-Beat Variability in Noisy Signals

Magnus Åström, *Student Member, IEEE*, Elena Carro Santos, Leif Sörnmo*, *Member, IEEE*, Pablo Laguna, *Member, IEEE*, and Björn Wohlfart

***Abstract*—The measurement of subtle morphologic beat-to-beat variability in the electrocardiogram (ECG)/vectorcardiogram (VCG) is complicated by the presence of noise which is caused by, e.g., respiration and muscular activity. A method was recently presented which reduces the influence of such noise by performing spatial and temporal alignment of VCG loops. The alignment is performed in terms of scaling, rotation and time synchronization of the loops. Using an ECG simulation model based on propagation of action potentials in cardiac tissue, the ability of the method to separate morphologic variability of physiological origin from respiratory activity was studied. Morphologic variability was created by introducing a random variation in action potential propagation between different compartments. The results indicate that the separation of these two activities can be done accurately at low to moderate noise levels (less than 10 μV). At high noise levels, the estimation of the rotation angles was found to break down in an abrupt manner. It was also shown that the breakdown noise level is strongly dependent on loop morphology; a planar loop corresponds to a lower breakdown noise level than does a nonplanar loop.**

***Index Terms*—ECG signal processing, morphologic beat-to-beat variability, noise performance, VCG loop alignment.**

I. Introduction

THE ALIGNMENT of vectorcardiographic (VCG) loops is useful in electrocardiographic (ECG) applications where joint analysis of two or more loops is of interest. For example, serial comparison of VCG recordings overcomes certain problems when combined with loop alignment which are commonly associated with the analysis of standard 12-lead ECG recordings [1], [2]. These problems include undesired shifts of the electrical axis caused by slight interrecording changes in, e.g., electrode positioning or body position which make the comparison of QRS waveform measurements more difficult.

The measurement of subtle beat-to-beat variations in QRS morphology is another example where loop alignment has been considered, primarily for the purpose of reducing the effects of respiration [3]. This type of variability measurement was originally suggested as a means for studying electrical instability of the heart. The variability was quantified as the ensemble variance of successive, time-aligned sinus beats, see, e.g., [4] and [5]; an increased variance was considered as an indicator of instability. In these earlier studies, methods for respiratory compensation were either neglected or compensated for in a rather basic fashion. Later, the importance of employing such compensation techniques was demonstrated: loop alignment sometimes reduced considerable morphologic variability to a value close to the variability of the noise [3]. Similar results were obtained using a lead-dependent, nonspatial compensation technique for the measurement of morphologic QRS variability [6].

Still another application of loop alignment is the cancellation of QRST complexes for the purpose of analyzing atrial fibrillation in the surface ECG/VCG [7]. This application is related to the measurement of morphologic beat-to-beat variability, however, the residual signal, i.e., the atrial fibrillation waves, is now the desired quantity rather than the aligned QRS waveforms. The residual signal is obtained by subtracting an aligned, averaged loop to each beat in the original ECG. It was found that loop alignment produces a signal with smaller QRS related residuals than does straightforward "averaged beat subtraction" and, as a result, the residual signal is much better suited for spectral analysis of the fibrillatory waveforms [8].

The present study investigates a number of issues which are related to the performance of VCG loop alignment and focus, in particular, on the maximum likelihood (ML) alignment method [3]. It is evident that the performance of loop alignment depends on the noise level and is likely to become inaccurate above a certain level. Few results, if any, have been presented in the literature which describe the performance in noise; this lack is probably due to that most studies involve ECG data acquired during rest and thus has a low noise level. Nevertheless, loop alignment is sometimes called for in noisy situations, e.g., for the purpose of QRST complex cancellation (see above) or for the analysis of data acquired during exercise. Furthermore, it is of interest to assess how loop morphology influences alignment performance at different noise levels. In this study, morphology is characterized by means of a measure related to how planar shape the loop

Manuscript received August 14, 1998; revised January 4, 2000. This work was supported by the Swedish National Board for Technical Development (NUTEK) under Grant no. 89-03 381P. *Asterisk indicates corresponding author*.

M. Åström is with the Signal Processing Group, Department of Applied Electronics, Lund University, S-221 00 Lund, Sweden.

E. Carro Santos is with the Signal Processing Group, Department of Applied Electronics, Lund University, S-221 00 Lund, Sweden. She is also with the Communication Technology Group, Department of Electronics Engineering and Communications, University of Zaragoza, 50015 Zaragoza, Spain.

*L. Sörnmo is with the Signal Processing Group, Department of Applied Electronics, Lund University, Box 118, S-221 00 Lund, Sweden (e-mail: leif.sornmo@tde.lth.se).

P. Laguna is with the Communication Technology Group, Department of Electronics Engineering and Communications, University of Zaragoza, 50015 Zaragoza, Spain.

B. Wohlfart is with the Department of Clinical Physiology, Lund University, S-221 00 Lund, Sweden.

Publisher Item Identifier S 0018-9294(00)02641-0.

exhibits. The properties of the estimated loop rotation matrix are studied in terms of rotation angles for different loop morphologies. A breakdown noise level is heuristically established for the angle estimates.

Another important aspect of loop alignment performance is related to the measurement of morphologic variability. Although techniques are necessary for separating, e.g., respiratory activity from variability of physiological origin, it remains to be shown whether this separation can be done accurately or at the expense of a distorted physiological variability. In order to study this aspect, an action potential model is here used for generating controlled morphologic variability of the body surface potentials [9], [10].

II. VCG Loop Alignment

This section summarizes the essentials of a recent method for spatiotemporal alignment of VCG loops [3]. The method is based on a statistical signal model in which it is assumed that an observed VCG loop of the QRS complex $\mathbf{Z}$ derives from a reference loop $\tilde{\mathbf{Z}}_R$ but has been altered by a series of transformations. The matrix $\mathbf{Z}$ is $3\times K$ with each row vector contains K samples of an ECG lead. The reference loop $\tilde{\mathbf{Z}}_R$ is $3\times(K+2\Delta)$ and has 2Δ additional samples in order to allow for observations which constitute different subsets of K samples from $\tilde{\mathbf{Z}}_R$. The tilde indicates that $\tilde{\mathbf{Z}}_R$ has been augmented with samples. The following three transformations are considered for modeling activities of extracardiac origin: *Scaling* by the positive-valued, parameter α allows for loop expansion or contraction; *rotational* changes of the heart which are due to, e.g., respiration are accounted for by the orthonormal, 3×3 matrix $\mathbf{Q}$ (it should be noted that the rotation matrix is fixed during the entire QRS interval); *time synchronization* is introduced in the signal model by the shift matrix $\mathbf{J}_\tau$. Due to the larger size of $\tilde{\mathbf{Z}}_R$, the observed loop $\mathbf{Z}$ can result from any of the $(2\Delta+1)$ possible positions in $\tilde{\mathbf{Z}}_R$. The shift matrix $\mathbf{J}_\tau$ is defined by the integer time shift τ

$$\mathbf{J}_\tau = \begin{bmatrix} \mathbf{0}_{\Delta+\tau} \\ \mathbf{I} \\ \mathbf{0}_{\Delta-\tau} \end{bmatrix} \tag{1}$$

where $\tau = -\Delta,\ldots,\Delta$. The dimensions of the top and bottom zero matrices in (1) are equal to $(\Delta+\tau)\times K$ and $(\Delta-\tau)\times K$, respectively. One of the zero matrices vanishes when τ is $\pm\Delta$. The identity matrix $\mathbf{I}$ is $K\times K$. The 2Δ samples of the reference loop are equally divided into samples prepended and appended to the QRS centered interval, respectively. The observation model for one beat is thus described by

$$\mathbf{Z} = \alpha\mathbf{Q}\tilde{\mathbf{Z}}_R\mathbf{J}_\tau + \mathbf{W} \tag{2}$$

where the transformed reference loop is assumed to be additively disturbed by white, Gaussian noise $\mathbf{W}$.

Maximum likelihood estimation has been applied to the problem of estimating the parameters that minimize the Euclidean distance between corresponding points of the VCG loops. The optimal estimates of α, $\mathbf{Q}$ and τ can be found by solving the following minimization problem

$$\epsilon^2_{\min} = \min_{\alpha,\mathbf{Q},\tau} ||\mathbf{Z} - \alpha\mathbf{Q}\tilde{\mathbf{Z}}_R\mathbf{J}_\tau||_F^2 \tag{3}$$

where the Frobenius norm for an $m\times n$ matrix $\mathbf{X}$ is defined by $||\mathbf{X}||_F^2 = \sum_{i=1}^m\sum_{j=1}^n |x_{ij}|^2$. The minimization in (3) is performed by first finding closed-form expressions for the estimates α and $\mathbf{Q}$ under the assumption that τ is fixed. The optimal estimates of α, τ, and $\mathbf{Q}$ are then determined by evaluating the error ϵ^2 for different values of τ in the interval $[-\Delta,\Delta]$. The resulting ML estimate of $\mathbf{Q}$ is given by [3]

$$\hat{\mathbf{Q}}_\tau = \mathbf{U}\mathbf{V}^T \tag{4}$$

where the columns of $\mathbf{U}$ and $\mathbf{V}$ are the left and right eigenvectors of the matrix $\mathbf{C} = \mathbf{Z}\mathbf{J}_\tau^T\tilde{\mathbf{Z}}_R^T$. The matrices $\mathbf{U}$ and $\mathbf{V}$ are obtained by singular value decomposition (SVD) of $\mathbf{C}$, i.e., $\mathbf{C} = \mathbf{U}\mathbf{\Sigma}\mathbf{V}^T$ (the diagonal matrix $\mathbf{\Sigma}$ contains the singular values). The index τ has been attached to $\hat{\mathbf{Q}}_\tau$ in (4) since this estimate is only optimal for one particular value of τ. The estimate of α can then be calculated since $\hat{\mathbf{Q}}_\tau$ is available

$$\hat{\alpha}_\tau = \frac{\mathrm{tr}\left(\mathbf{Z}^T\hat{\mathbf{Q}}_\tau\tilde{\mathbf{Z}}_R\mathbf{J}_\tau\right)}{\mathrm{tr}\left(\mathbf{J}_\tau^T\tilde{\mathbf{Z}}_R^T\tilde{\mathbf{Z}}_R\mathbf{J}_\tau\right)} \tag{5}$$

where tr denotes the matrix trace. The time synchronization parameter τ is estimated by means of a grid search for the allowed set of values

$$\hat{\tau} = \arg\min_\tau ||\mathbf{Z} - \hat{\alpha}_\tau\hat{\mathbf{Q}}_\tau\mathbf{Z}_R\mathbf{J}_\tau||_F^2. \tag{6}$$

The estimate $\hat{\tau}$ is then used to determine which of the estimates in the set of estimates $\hat{\alpha}_\tau$ and $\hat{\mathbf{Q}}_\tau$ that should be selected to yield $\hat{\alpha}$ and $\hat{\mathbf{Q}}$.

The above loop alignment technique requires that the reference loop $\tilde{\mathbf{Z}}_R$ is available *a priori* for alignment to the observed loop $\mathbf{Z}$. In this study, $\tilde{\mathbf{Z}}_R$ is simply selected as the first loop of the loops available for alignment. Another approach of choosing $\tilde{\mathbf{Z}}_R$ is, e.g., updating it recursively among already aligned beats. With these choices of $\tilde{\mathbf{Z}}_R$, it is obvious that the alignment of $\tilde{\mathbf{Z}}_R$ to $\mathbf{Z}$, as described by (3), can be done in a dual manner by instead aligning $\mathbf{Z}$ to $\tilde{\mathbf{Z}}_R$. In the following, each observed loop is, therefore, aligned to $\tilde{\mathbf{Z}}_R$ and considered for further morphologic analysis after compensation by the estimated transformation parameters (the definition of $\tilde{\mathbf{Z}}_R$ and the dual alignment was discussed in more detail in [3]).

The three rotation angles can be obtained from the estimated rotation matrix $\hat{\mathbf{Q}}$ by viewing this matrix as a product of three planar rotations. It is shown that angle estimates can be obtained by [3]

$$\hat{\varphi}_Y = \arcsin(\hat{q}_{1,3}) \tag{7}$$

$$\hat{\varphi}_X = \arcsin\left(\frac{\hat{q}_{1,2}}{\cos\hat{\varphi}_Y}\right) \tag{8}$$

$$\hat{\varphi}_Z = \arcsin\left(\frac{\hat{q}_{2,3}}{\cos\hat{\varphi}_Y}\right). \tag{9}$$

where $\hat{q}_{m,n}$ denotes element (m,n) of $\hat{\mathbf{Q}}$.

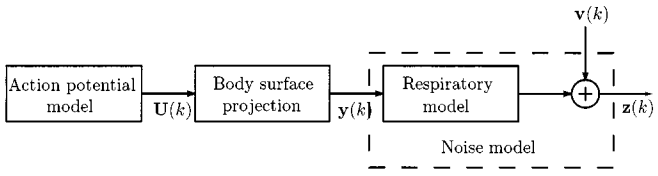

Fig. 1. Block diagram of the cardiac simulation model.

III. Signals for Performance Assessment

Both simulated and recorded ECG signals were employed for assessing the performance of ML loop alignment. In particular, the simulation approach was adopted since it allowed better control of the degree of morphologic beat-to-beat variability.

A. Simulation Model

The main blocks of the simulation model are presented below (Fig. 1). The cardiac action potential model was originally developed by Wohlfart in a time continuous framework [9] but was later recast into matrix formulation better suited for computer simulation [11]. A very brief description of the action potential model is here provided with the primary aim to introduce the parameter controling morphologic variability; a complete description of the model is found elsewhere [9]–[11].

1) Action Potential Model—Morphologic Beat-to-Beat Variability: The propagation of action potentials in cardiac tissue is represented by a matrix of $M \times N$ elements which represents a two-dimensional model of the heart wall (M and N refer to the width and length of the wall, respectively)

$$\mathbf{U}(k) = \begin{bmatrix} u_{1,1}(k) & \cdots & u_{1,N}(k) \\ \vdots & \ddots & \vdots \\ u_{M,1}(k) & \cdots & u_{M,N}(k) \end{bmatrix} = \begin{bmatrix} \mathbf{u}_1(k) \\ \vdots \\ \mathbf{u}_M(k) \end{bmatrix} \quad (10)$$

where $u_{m,n}(k)$ is the membrane potential at sample k of the (m,n)th compartment. The top and bottom row, $\mathbf{u}_1(k)$ and $\mathbf{u}_M(k)$, represent the potentials of the endo- and epicardium, respectively.

Action potentials are simulated by means of ion currents, stimulus currents and intercompartmental currents considering the states of cell activation and inactivation and membrane potential differences. Within this context, morphologic beat-to-beat variability is introduced in the model, (11) found at the bottom of the page, by assuming that the intercompartmental current $\mathbf{j}_i(k)$ is proportional to the voltage difference between two adjacent compartments in the same column. Here, the function $\beta_i(k)$ can be viewed as a time-varying conductivity between the endo- and the epicardium and is modeled by a random sequence of uncorrelated, Gaussian variables

$$\beta_i(k) \in N(m_\beta, \sigma_\beta). \quad (12)$$

2) Body Surface Potentials: Since the relationship between electrical excitation of cardiac tissue and body surface potentials is complex, a simplified approach is used in which body surface potentials are linearly related to the potential differences between the endo- and epicardium. The surface leads $\mathbf{y}(k)$ (3×1) are obtained by

$$\mathbf{y}(k) = \mathbf{P}(\mathbf{u}_1(k) - \mathbf{u}_M(k))^T \quad (13)$$

where the $\mathbf{P}$ matrix $(3 \times K)$ projects the potential differences onto the leads in the vector $\mathbf{y}(k)$ that is a three element vector representing the VCG signal. In practice, the projection matrix $\mathbf{P}$ is unknown and, therefore, has to be estimated. This can be done by reversing the above procedure: knowledge of the surface leads and the membrane potential differences can be used to infer $\mathbf{P}$ [11].

In this study, $\mathbf{P}$ is determined such that the leads $\mathbf{y}(k)$ closely resembled those of an orthogonal VCG lead configuration (X, Y, Z) recorded from a healthy subject, see Fig. 2(a); this particular choice of $\mathbf{P}$ is used for the performance assessment presented in Sections IV-A and IV-B.

3) Noise Model: The simulation model is extended to account for noise of extracardiac origin, e.g., due to respiration and muscular activity. Such modeling is done, similar to the loop alignment model in (2), by assuming that the leads $\mathbf{y}(k)$ in (13) are transformed by scaling and rotation but now on a *sample-to-sample* basis

$$\mathbf{z}(k) = \alpha(k)\mathbf{Q}(k)\mathbf{y}(k) + \mathbf{v}(k). \quad (14)$$

The matrix $\mathbf{Q}(k)$ can be computed as the product of planar rotations with time-varying angles [11]. It is assumed that angular variation is proportional to the amount of air in the lungs during a respiratory cycle, a property which is modeled as the product of two sigmoidal functions reflecting inhalation and exhalation, respectively. The angular variation around lead X is defined by

$$\varphi_X(k) = \eta_X \left(\frac{1}{1+e^{\lambda_i(k-\kappa_i)}}\right)\left(\frac{1}{1+e^{\lambda_e(k-\kappa_e)}}\right) \quad (15)$$

where the duration of inspiration and expiration is determined by the parameters λ_i and λ_e, respectively. Another pair of parameters, κ_i and κ_e, describe the time delays of the sigmoidal functions. The inhalation and exhalation become separated in time when κ_e is different from κ_i. The parameter η_X defines the range of the angle variation. Similar variational patterns can naturally be defined for leads Y and Z, however, these rotation

$$\mathbf{j}_i(k) = \begin{cases} \beta_i(k)(\mathbf{u}_{i+1}(k) - \mathbf{u}_i(k)) & i = 1 \\ \beta_i(k)((\mathbf{u}_{i+1}(k) - \mathbf{u}_i(k)) + (\mathbf{u}_{i-1}(k) - \mathbf{u}_i(k))) & i = 2, \ldots, M-1 \\ \beta_i(k)(\mathbf{u}_{i-1}(k) - \mathbf{u}_i(k)) & i = M \end{cases} \quad (11)$$

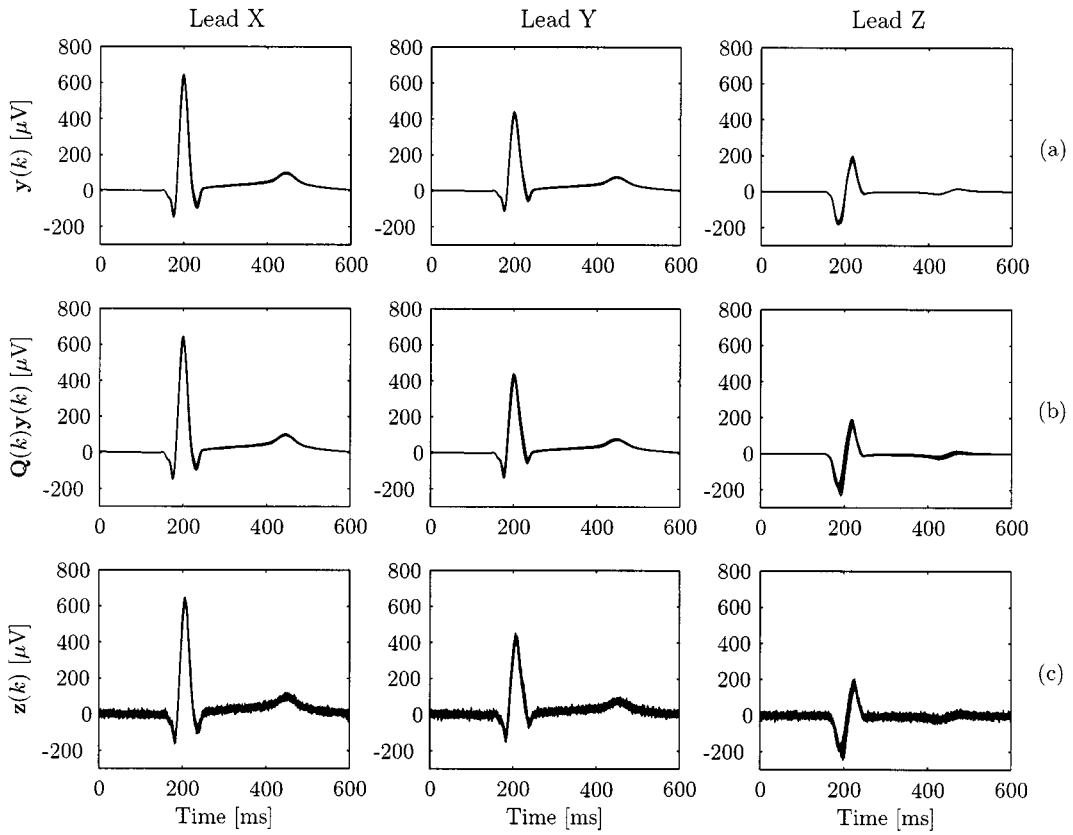

Fig. 2. Morphologic variability shown as 50 superimposed beats (a) of the simulated signal $\mathbf{y}(k)$ ($\sigma_\beta = 0.0025$), (b) after rotation around the X-axis ($\eta_X = 15°$), and (c) after white noise has been added ($\sigma_v = 10\mu$V).

angles were set to zero. The sigmoidal pattern is defined by the following parameter setup:

$$\lambda_i = -20\frac{f_r}{f_s}, \quad \kappa_i = 0.35\frac{f_s}{f_r}, \quad \lambda_e = 15\frac{f_r}{f_s},$$
$$\kappa_e = 0.6\frac{f_s}{fr},$$

The respiratory rate f_r is set to 0.2 Hz and the sampling rate f_s to 1000 Hz. The scale factor $\alpha(k)$ in (14) is set to unity at all times in this study. The additive noise $\mathbf{v}(k)$ is assumed to be a white, Gaussian process with variance σ_v^2 and has no interlead correlation.

Fig. 2(b) presents the combined effect of morphologic variability and rotation, as introduced by σ_β and $\mathbf{Q}(k)$, respectively. Since rotation takes place around the X axis, only leads Y and Z are influenced. Finally, Fig. 2(c) shows the end result of the simulation model.

B. ECG Database

The effects of loop morphology on the alignment process were investigated by means of a database containing subjects referred for myocardial scintigraphy [12]. Thirty-four subjects without any signs of ischemia or infarction were included for this study. The ECG signals were recorded during rest for 5 min using a standard 12-lead configuration. The acquisition was done at a sampling rate of 1000 Hz using equipment by Siemens-Elema AB, Solna, Sweden. The VCG signal was synthesized by linear combination of the 12 leads using the inverse Dower weighting matrix [13]. For each subject, an average beat was computed from normal sinus beats in order to obtain a low noise level of the reference loop.

IV. Performance of VCG Loop Alignment

The performance of the alignment method is evaluated below in terms of removing extracardiac noise in the presence of morphologic variability (Section IV-A), accuracy of alignment parameter estimates (Section IV-B) and sensitivity to various loop morphologies (Section IV-C). Results presented in Sections IV-A and IV-B derive from the simulation model while results in Section IV-C are based on the ECG database.

A. Morphologic Beat-to-Beat Variability

1) Performance Measures: The effect of loop alignment is studied by means of performance measures which reflect morphologic variability in relation to a reference beat. These measures are computed for beats at different stages of the simulation model: for 1) noise-free beats (i.e., before white noise has been added), 2.) noisy beats, and 3) aligned beats. Starting with the measure at the third stage, this measure reflects sample-to-sample morphologic variability after loop alignment and is defined by

$$\varsigma_{\hat{\mathbf{y}}}^2(k) = \frac{1}{B}\sum_{i=1}^{B}(\hat{\mathbf{y}}_i(k) - \bar{\mathbf{y}}(k))^2 \tag{16}$$

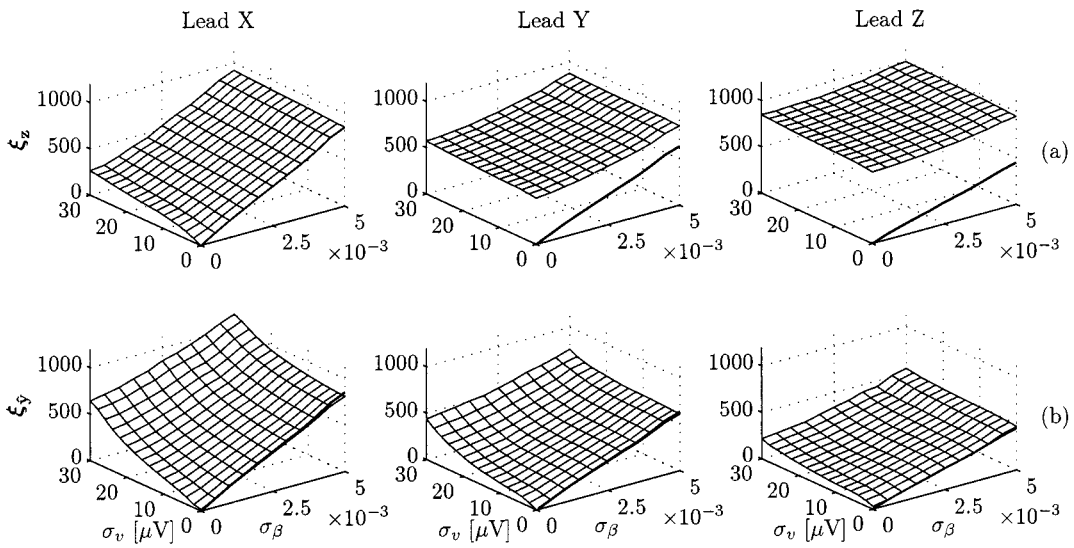

Fig. 3. Morphologic QRS variability of (a) noisy beats $\xi_{\mathbf{z}}$ and (b) aligned beats $\xi_{\hat{\mathbf{y}}}$ [cf. (19)]. The variability of the noise-free beats $\xi_{\mathbf{y}}$ is plotted as a solid line for $\sigma_v = 0$ μV.

where B is the number of beats ($B = 500$), $\hat{\mathbf{y}}_i(k)$ the ith beat of the aligned signal and $\bar{\mathbf{y}}(k)$ is the reference beat (which here is taken as the average of the noise-free beats, cf. [4] and [12]). It should be noted that the quantities in (16) are vector-valued. In order to compare morphologic variability at different noise levels, the noise variance should first be estimated and corrected for in each lead. An estimate of the noise variance is obtained by

$$\hat{\sigma}^2_{v,\hat{\mathbf{y}}} = \frac{1}{I_Q}\frac{1}{B}\sum_{k=1}^{L}\sum_{i=1}^{B}(\hat{\mathbf{y}}_i(k) - \bar{\mathbf{y}}(k))^2. \tag{17}$$

The interval was located before the Q wave onset (I_Q was set to 50 ms) since it essentially contains variability due to noise. The noise-corrected variability function is then defined by

$$\psi_{\hat{\mathbf{y}}}(k) = \sqrt{\varsigma^2_{\hat{\mathbf{y}}}(k) - \hat{\sigma}^2_{v,\hat{\mathbf{y}}}}. \tag{18}$$

Finally, the over-all measure of morphologic QRS variability is obtained by summation of $\psi_{\hat{\mathbf{y}}}(k)$ during the QRS interval

$$\xi_{\hat{\mathbf{y}}} = \sum_{k\in \mathrm{QRS}} \psi_{\hat{\mathbf{y}}}(k). \tag{19}$$

For the noise-free and the noisy beats, morphologic variability is computed in a similar way and the subindexes $\mathbf{y}$ and $\mathbf{z}$ are attached instead (evidently an estimate of the noise variance is not required for the first measure).

2) Results: Morphologic variability before and after loop alignment was investigated in relation to the noise level σ_v and the morphologic variability σ_β, see Fig. 3. As reference value, the same measurements for the noise-free beats are plotted as a solid line in Fig. 3(a) and (b).

In the upper panel, the morphologic variability before alignment is a combination of physiological effects, rotation and additive noise. The variability, $\xi_{\mathbf{z}}$, in leads Y and Z is larger than in lead X because of the rotation around the X axis only. In the bottom panel, it is obvious that the variability due to rotation can be essentially removed at low to moderate noise levels while beat-to-beat variability caused by σ_β remains. It should be noted that $\xi_{\mathbf{z}}$ and $\xi_{\hat{\mathbf{y}}}$ in Fig. 3(a)–(b) have been corrected by subtraction of the noise variance. Therefore, the increase in $\xi_{\hat{\mathbf{y}}}$ at increasing noise levels is essentially due to less accurate alignment.

Two examples of different morphologic variability are studied in further detail (Figs. 4 and 5). The first case has a low noise level and low morphologic variability. In this case, variability due to rotation is removed from the aligned beats while the morphologic variability of the noise-free beats remains. The second case contains beats with considerable morphologic variability at a high noise level, see Fig. 5. The effect of rotation is again considerably reduced by alignment, however, the sample-to-sample variability of the aligned beats no longer coincides with that of the noise-free beats, cf. Figs. 4(d) and 5(d).

B. Estimation of Alignment Parameters

Rotation angles can be derived from the estimated rotation matrix $\hat{\mathbf{Q}}$. The results presented below are similar to those in Sections III in the sense that the estimated angles are compared to the ones of the model at different levels of morphologic variability and noise.

1) Performance Measures: In the alignment method, the rotation matrix is estimated only once for the ith beat ($\hat{\mathbf{Q}}_i$ and the related $\hat{\varphi}_{X,i}$, $\hat{\varphi}_{Y,i}$ and $\hat{\varphi}_{Z,i}$) while the rotation of the simulation model is a time-varying function, i.e., $\mathbf{Q}(k)$, $\varphi_X(k)$, $\varphi_Y(k)$ and $\varphi_Z(k)$. In order to compare these two quantities, the average of the model rotation angles during the ith QRS complex, $\bar{\varphi}_i$, is used as reference value. The error measure for the angle estimates is given by

$$\delta_{\hat{\varphi}} = \sqrt{\frac{1}{B}\sum_{i=1}^{B}(\hat{\varphi}_i - \bar{\varphi}_i)^2} \tag{20}$$

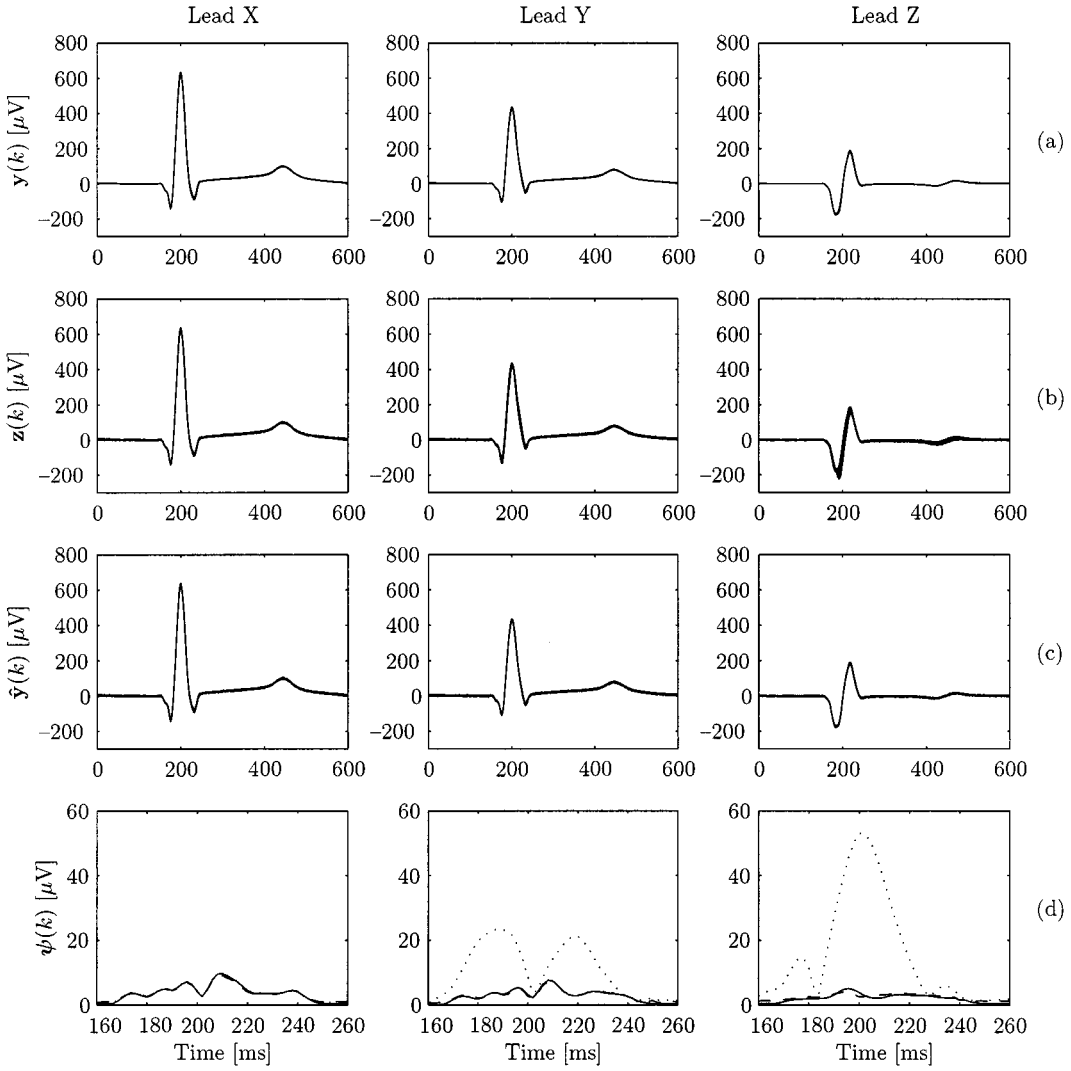

Fig. 4. An example of small morphologic variability and low noise level ($\sigma_\beta = 0.001$, $\sigma_v = 2\ \mu$V). (a) Noise-free beats. (b) Noisy beats. (c) Aligned beats. (d) Corresponding QRS variability for the beats in (a), (b), and (c) plotted with solid, dotted, and dashed line, respectively. Note that the time scale is magnified (d) during the QRS interval.

where $\hat{\varphi}_i = [\hat{\varphi}_{X,i}\ \hat{\varphi}_{Y,i}\ \hat{\varphi}_{Z,i}]^T$. It should be noted that a small error is always present in (20) due to the once-per-beat estimate of the loop alignment method. Fortunately, this error is negligible except for when extremely rapid changes occur in the rotation angles.

In the same way, the accuracy of the scale factor estimate $\hat{\alpha}_i$ can be judged by comparison to the average value $\bar{\alpha}_i$ as obtained from the model scale function $\alpha(k)$. The resulting error measure is denoted with $\delta_{\hat{\alpha}}$ and is a scalar version of the definition in (20).

2) Results: The resulting error measure $\delta_{\hat{\varphi}}$ for the angle estimation is presented in Fig. 6(a) for different degrees of morphologic variability, σ_β, and noise levels, σ_v. An interesting behavior can be observed in lead Z where a distinct noise level exists above which the performance rapidly deteriorates and estimates with large variance result. Here, this level is referred to as the *breakdown noise level*. This behavior can also be observed in the other leads but the decrease in performance is not as drastic as in lead Z.

The accuracy of the estimated scale factor is presented in Fig. 6(b). In contrast to the angle estimates, no sharp increase in $\delta_{\hat{\alpha}}$ can be observed at higher noise levels but instead the increase is rather gradual. However, the results in Fig. 6(b) indicate that the scale factor estimate becomes biased at high noise levels and that $\hat{\alpha}$ decreases, in general, for an increasing σ_v. It should be recalled that $\alpha(k)$ was identical to one in the simulation model at all times.

For a somewhat higher noise level ($\sigma_v = 16\ \mu$V), it is apparent that the estimated rotation angles follow the true values very well, see Fig. 7(a). For a slightly increased noise level ($\sigma_v = 24\ \mu$V), however, the rotation is no longer reliable for all beats, see Fig. 7(b). In such cases, anomalous angle estimates result at various points in time [at 11, 14, and 19 s in Fig. 7(b)].

C. Dependence on Loop Morphology

An interesting extension of the results presented in Sections IV-A and IV-B is to investigate the relationship between loop morphology and breakdown noise level. This relationship is

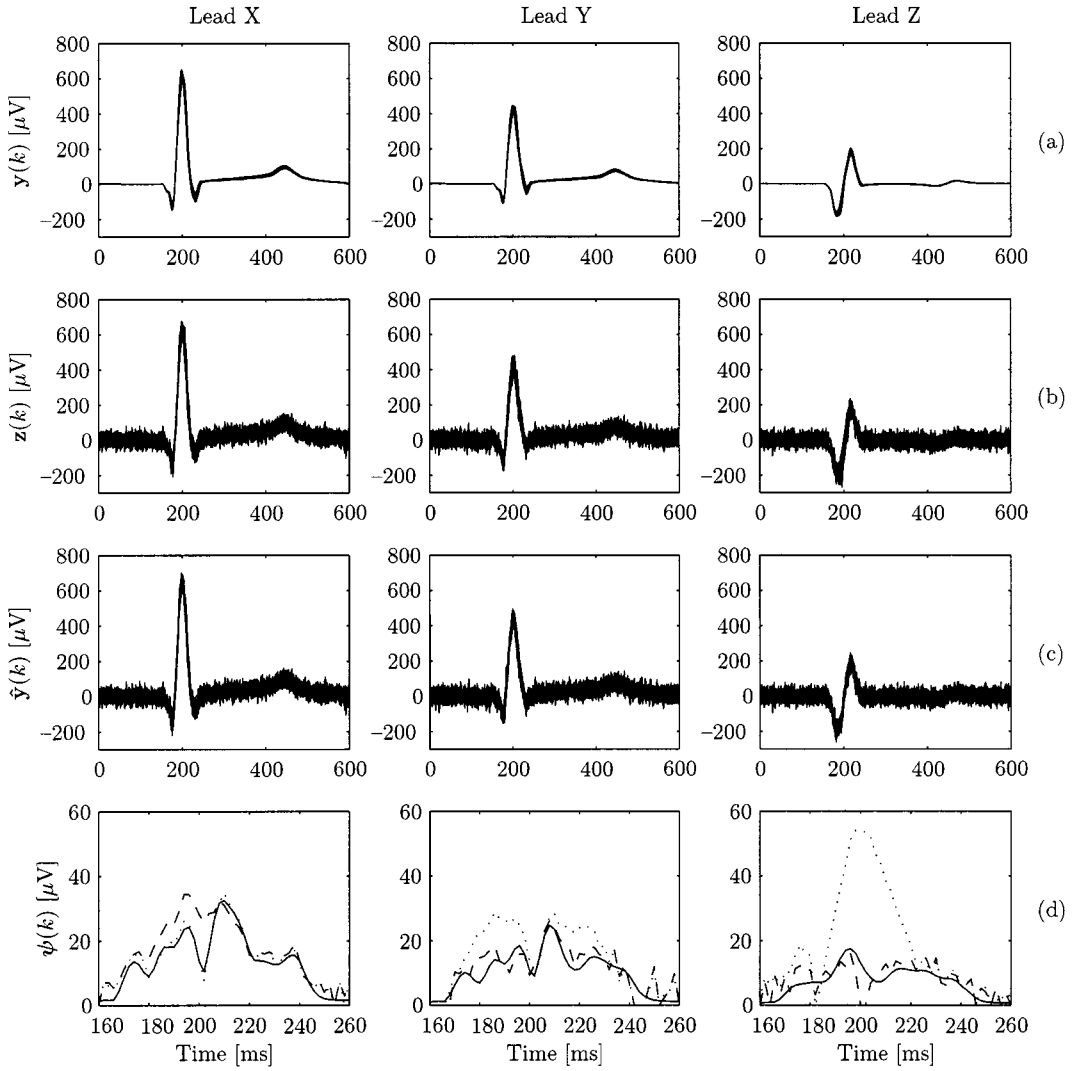

Fig. 5. An example of large morphologic variability and moderate noise level ($\sigma_\beta = 0.004$ and $\sigma_v = 24$ μV); see Fig. 4 for further details.

here pinpointed by use of the ECG database where various degrees of white noise has been added to each averaged beat.[1]

1) Performance Measure: Loop morphology was characterized by an over-all measure reflecting the planarity of a loop. This measure is defined as the ratio between the minimum and the maximum singular values of the VCG loop matrix

$$\rho = \frac{\sigma_{\min}}{\sigma_{\max}}. \tag{21}$$

The limiting values of ρ are zero and one which, thus, correspond to an entirely planar loop and a loop which extends equally into all three dimensions, respectively.

The breakdown noise level $\tilde{\sigma}_v$ is taken as that noise level which produces angle estimation errors which in each lead exceed a certain threshold value χ. The vector definition of these noise levels is given by

$$\tilde{\sigma}_v = \arg\min_{\sigma_v} |\boldsymbol{\Delta}\hat{\varphi}_{\sigma_v} - \chi\mathbf{1}| \tag{22}$$

[1]Each loop in the database was normalized using the Frobenius norm in order to reduce the influence of differences in signal-to-noise ratio.

where the maximum error, $\boldsymbol{\Delta}\hat{\varphi}_{\sigma_v}$, is

$$\boldsymbol{\Delta}\hat{\varphi}_{\sigma_v} = \max_i |\hat{\varphi}_{i,\sigma_v} - \bar{\varphi}_{i,\sigma_v}| \tag{23}$$

and $\mathbf{1}$ is a vector with all elements equal to one. The choice of threshold value χ was based on the observation that the error $\boldsymbol{\Delta}\hat{\varphi}_{\sigma_v}$ is small below a certain noise level while then rapidly increasing to a considerably larger error value. By setting χ equal to $\pi/10$, the noise level at which angle estimates became anomalous was accurately identified. The noise level σ_v was incremented in steps of 5 μV.

2) Results: Fig. 8 shows that the accuracy of loop alignment is strongly dependent on loop morphology since the breakdown noise level ranges from 5 μV to 70 μV. It should be noted that the breakdown noise level is selected from the lead with the lowest level. These results also suggest that an essentially linear relationship exists between loop planarity and breakdown noise level. Fig. 9 exemplifies the range of this level by means of two loops with high and low degree of planarity, respectively, and accordingly a low and high breakdown noise level, respectively. It is obvious from Fig. 9(a) that the planar loop is almost entirely

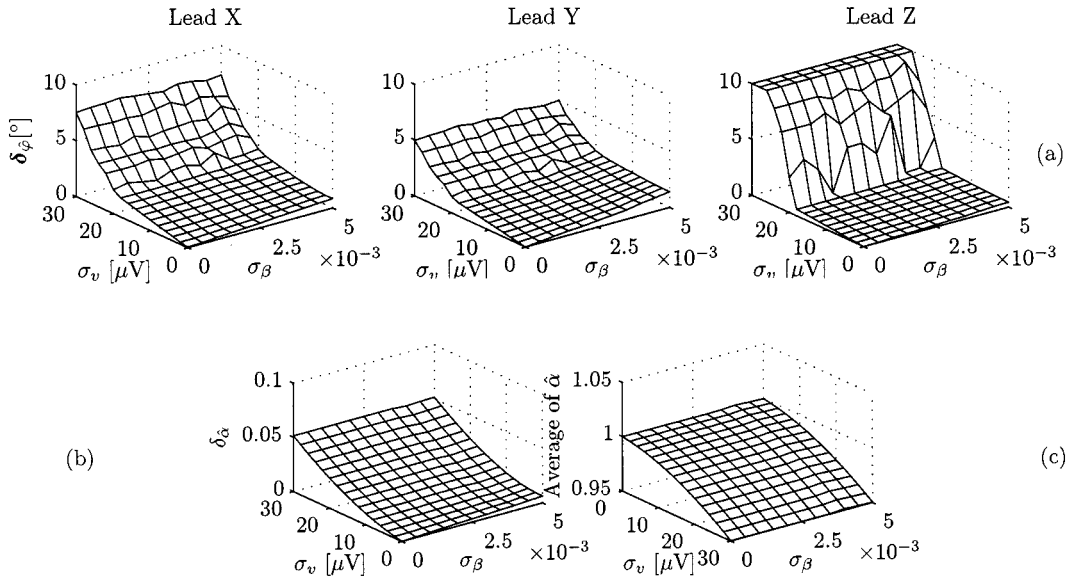

Fig. 6. Error measures for (a) rotation angle estimates and (b) scale factor estimates as functions of σ_β and σ_v. (c) The average of the scale factor estimates (note that the noise level σ_v is shown in reversed order to simplify the interpretation of the diagram).

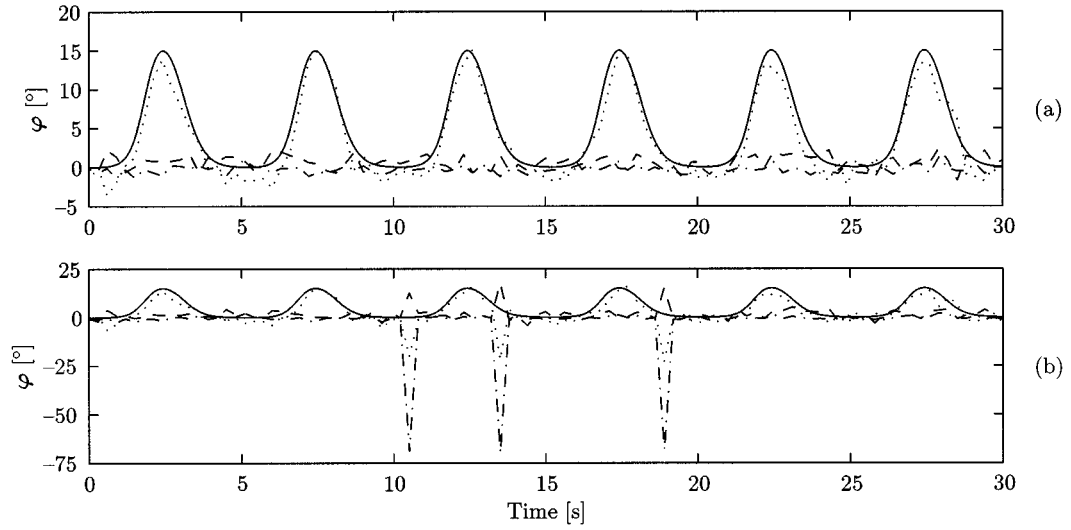

Fig. 7. Estimation of rotation angles at differing noise levels. (a) Angle estimates from leads X, Y, and Z are shown with dotted, dashed, and dash-dotted line, respectively, for $\sigma_v = 16$ μV. (b) As in (a) but with $\sigma_v = 24$ μV. The morphologic variability was set to $\sigma_\beta = 0.004$. The solid line shows the original angle variation in lead X. Note that the scales of the vertical axes in (a) and (b) differ.

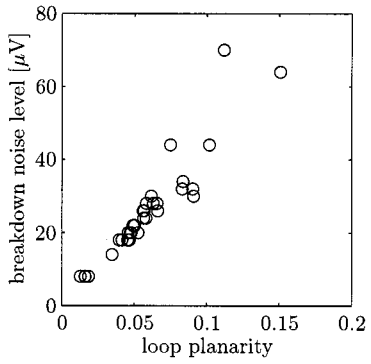

Fig. 8. Breakdown noise level as a function of loop planarity. Note that the breakdown noise level is taken from the lead with the lowest level.

inscribed by two dimensions due to an almost linear dependence between the transformed leads X' and Y' (the transformation is explained in the figure text). In Fig. 9(b), the loop extends into all three dimensions and, accordingly, the corresponding breakdown noise level is much higher than for the case in Fig. 9(a).

V. Discussion

A. Simulation Model

An important advantage with the simulation approach is that the morphologic QRS variability is assigned a parametric description, here introduced by the parameter σ_β. This property

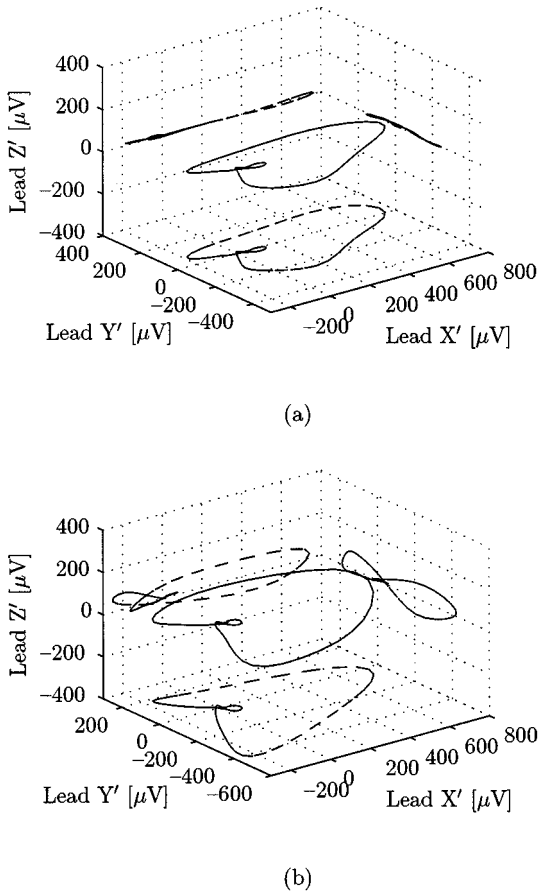

Fig. 9. VCG loops with (a) a low ρ ($\rho = 0.015$) and (b) a high ρ ($\rho = 0.12$). The loops have been rotated to their singular planes where X', Y', and Z' corresponds to the axes of the singular values in decreasing order.

is critical when assessing the compensation of, e.g., respiratory activity in the presence of morphologic variability. Several, rather complex models of cardiac action potentials have been described in the literature, see, e.g., [14]. The action potential model in [9] was considered suitable because of its simplicity and its modest computational demand while still providing sufficient waveform fidelity for the present purpose.

The effects of respiration were described by a sigmoidal variation pattern of the rotation angles assumed to reflect changes in lung volume during inspiration/expiration. Several alternatives to that pattern were investigated but did not produce results which differed significantly from those presented here. For example, other angular patterns, e.g., a sinusoidal one, were studied as well as the effect of increasing respiratory rates, ranging up to 30 breaths/min, but these modifications had negligible influence on the various performance measures. Rotation was introduced around the X axis only, however, from a mathematical point of view there is no fundamental difference between rotation in one or in several leads when performing the SVD. As a consequence, rotation in several leads does not produce results which differ from those of a single lead.

B. Morphologic Variability

The measurements presented in Fig. 3 clearly showed that variability due to respiration was substantially reduced by loop alignment while the underlying morphologic QRS variability was not much influenced. At high noise levels, the variability measurements, $\xi_{\hat{\mathbf{y}}}$, became biased because the performance of the loop alignment method deteriorated. This property is, of course, closely related to the breakdown of the angle estimates as characterized by the diagrams in Fig. 6(a). However, it should be noted that measurements on morphologic variability does not exhibit a breakdown noise level as striking as that of the angle estimates, cf. Fig. 3(b) versus Fig. 6(a).

Although the results on morphologic variability were based on only one particular loop morphology (selected from a normal subject), a wide range of other morphologies can easily be simulated by means of different body surface projection matrices $\mathbf{P}$. The variability measures $\xi_{\hat{\mathbf{y}}}$ and $\delta_{\hat{\varphi}}$ were computed for several other morphologies but only the latter measure turned out to possess a strong dependence on morphology; further results related to $\xi_{\hat{\mathbf{y}}}$ were, therefore, omitted.

C. Loop Morphology

Although VCG loop alignment has been investigated within several contexts in the literature, the relationship between loop morphology and noise level established in Section IV-C appears to be new. By using a measure related to loop planarity, it was demonstrated that the alignment breakdown noise level had an essentially linear dependence on loop planarity, cf. Fig. 8. This result thus implies that the measurement of noise level and loop planarity can be motivated for prediction of loop alignment reliability.

Normal subjects have VCG loops which, in general, are more planar than those of, e.g., patients with myocardial infarction. It is well-known that myocardial damage is often associated with loops which include bites, abnormal transitions or sharp edges which makes the loop less planar [15]. Therefore, such differences in loop characteristics imply that alignment can be expected to be more robust in infarct patients than in normal subjects. The results presented in Section IV-C are of limited value since they are based on a rather small database.

Although the effects of a time-dependent scale factor, $\alpha(k)$, were not explicitly studied, important insights of the properties of $\hat{\alpha}$ were, nevertheless, inferred when $\alpha(k)$ was set to one in the noise model. Most notably, it was found that $\hat{\alpha}$ became increasingly biased (underestimated) as the noise level σ_v increased. It remains to be explained what causes the bias in $\hat{\alpha}$.

REFERENCES

[1] J. Fayn, P. Rubel, and P. Arnaud, "A new methodology for optimal comparison of serial vectorcardiograms," *Comput. Cardiol.*, pp. 467–470, 1983.

[2] P. Rubel, J. Fayn, J. L. Willems, and C. Zywietz, "New trends in serial ECG analysis," *J. Electrocardiol.*, vol. 26, pp. 122–128, 1993. (Suppl.).

[3] L. Sörnmo, "Vectorcardiographic loop alignment and morphologic beat-to-beat variability," *IEEE Trans. Biomed. Eng.*, vol. 45, pp. 1401–1413, Dec. 1998.

[4] K. Prasad and M. Gupta, "Phase-invariant signature algorithm. A non-invasive technique for early detection and quantification of Ouabain-induced cardiac disorders," *Angiology*, vol. 30, pp. 721–732, 1979.

[5] S. Ben-Haim, A. Gil, Y. Edoute, M. Kochanovski, O. Azaira, E. Kaplinsky, and Y. Palti, "Beat to beat variation in healed myocardial infarction," *Amer. J. Cardiol.*, vol. 68, pp. 725–728, 1991.

[6] G. Shaw and P. Savard, "On the detection of QRS variations in the ECG," *IEEE Trans. Biomed. Eng.*, vol. 42, pp. 736–741, July 1995.

[7] M. Holm, S. Pehrson, M. Ingemansson, L. Sörnmo, R. Johansson, L. Sandhall, M. Sunemark, B. Smideberg, C. Olsson, and S. Olsson, "Non-invasive assessment of atrial refractoriness during atrial fibrillation in man—Introducing, validating and illustrating a new ECG method," *Cardiovasc. Res.*, vol. 38, pp. 69–81, 1998.
[8] M. Stridh and L. Sörnmo, "Spatiotemporal QRST cancellation techniques in the surface ECG for improved characterization of atrial fibrillation," *IEEE Trans. Biomed. Eng.*, to be published.
[9] B. Wohlfart, "Simulation of ECG from two pairs of action potentials," *Clin. Physiol.*, vol. 13, pp. 453–467, 1993.
[10] B. Wohlfart and P. Arlock, "Simulation of the electrogram for ion currents," *Clin. Physiol.*, vol. 13, pp. 441–451, 1993.
[11] M. Åström, E. Carro, L. Sörnmo, and B. Wohlfart. (1998) "Optimal alignment of vectorcardiographic loops, morphologic beat-to-beat variability and the presence of noise". Signal Processing Rep. SPR-42, Lund Univ., Lund, Sweden. [Online]. Available: HTTP: http://www.tde.lth.se
[12] L. Sörnmo, B. Wohlfart, J. Berg, and O. Pahlm, "Beat-to-beat QRS variability in the 12-lead ECG and the detection of coronary artery disease," *J. Electrocardiol.*, vol. 31, pp. 336–344, 1998.
[13] L. Edenbrandt and O. Pahlm, "Vectorcardiogram synthesized from a 12-lead ECG: Superiority of the inverse Dower matrix," *J. Electrocardiol.*, vol. 21, pp. 361–367, 1988.
[14] J. Malmivuo and R. Plonsey, *Bioelectromagnetism*. Oxford, U.K.: Oxford Univ. Press, 1995.
[15] P. M. MacFarlane, L. Edenbrandt, and O. Pahlm, *12-Lead Vectorcardiography*. Oxford, U.K.: Butterworth-Heinemann, 1994.

Magnus Åström (S'97) received the M.Sc. degree in electrical engineering in 1997 from Lund University, Lund, Sweden. He joined the Department of Applied Electronics in 1997 where he is presently working toward the Ph.D. degree.

His research interests is focused on signal processing with applications to cardiac electrical signals and hardware implementation aspects of signal processing algorithms.

Mr. Åström has been an elected member of the department board since 1998.

Elena Carro Santos was born in Soria, Spain. She received the M.Sc. degree in telecommunication engineering from the University of Zaragoza, Zaragoza, Spain, in 1997.

She was employed as a Research Engineer at Lund University in cooperation with the Department of Electronics Engineering and Communications at the University of Zaragoza from 1996 to 1998. She is now working with development of telecommunication systems for Siemens AG, Zaragoza, Spain. Her research interests include biomedical signal processing, especially problems related to ECG signal processing.

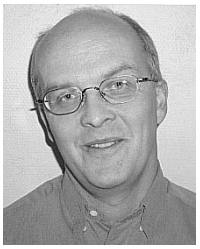

Leif Sörnmo (S'80–M'85) was born in Nässjö, Sweden, in 1955. He received the M.Sc. and D.Sc. degrees in electrical engineering from Lund University, Lund, Sweden, in 1978 and 1984, respectively.

He held a part-time position with the Department of Clinical Physiology, Lund University, from 1983 to 1995, working with computer-based ECG analysis. Since 1989, he has been an Associate Professor at the Signal Processing Group, Department of Applied Electronics, Lund University. His research interests include statistical signal processing and its application to the modeling and analysis of biomedical signals. His recent projects include spatiotemporal methods for detection of myocardial ischemia and time-frequency analysis of atrial fibrillation.

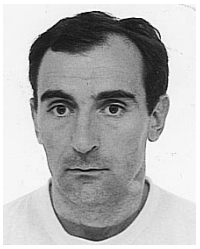

Pablo Laguna (M'92) was born in Jaca (Huesca), Spain, in 1962. He received the M.S. degree in physics and the Ph.D. degree from the University of Zaragoza (U.Z.), Zaragoza, Spain, in 1985 and 1990, respectively. The Ph.D. dissertation was developed at the Biomedical Engineering Division of the Institute of Cybernetics (I.C.), Politecnic University of Catalonia (U.P.C.)—C.S.I.C., Barcelona, Spain.

Since 1992, he has been an Associate Professor of Signal Processing and Communications in the Department of Electronics Engineering and Communications at the Centro Politecnico Superior, U.Z. From 1987 to 1992, he worked as Assistant Professor in the Department of Control Engineering at the U.P.C., and as a Researcher at the Biomedical Engineering Division of the I.C. His professional research interests are in signal processing, in particular applied to biomedical applications.

Björn Wohlfart received the Ph.D. and M.D. degrees from Lund University, Lund, Sweden, in 1982 and 1986, respectively.

Since 1990, he has been an Associate Professor with the Department Clinical Physiology, Lund University. His research interest is in basic inotropic and electrophysiologic mechanisms of the heart. His cardiac experiments are performed on Langendorf preparations, isolated trabeculae, and isolated myocytes. He is also working with computer simulations of cardiac electrophysiology.